

1 Efficiency and heat transport processes of low-temperature aquifer
2 thermal energy storage systems: new insights from global sensitivity
3 analyses

4
5 **Luka Tas¹, Niels Hartog^{2,3}, Martin Bloemendal⁴, David Simpson⁵, Tanguy Robert⁶, Robin Thibaut^{1,7},**
6 **Le Zhang¹, Thomas Hermans¹**

7 ¹Laboratory for Applied Geology and Hydrogeology, Department of Geology, Ghent University, Ghent,
8 Belgium

9 ²KWR, Water Research Institute, Nieuwegein, The Netherlands

10 ³Faculty of Geosciences, Utrecht University, Utrecht, The Netherlands

11 ⁴Department of Water Management, Delft University of Technology, Delft, The Netherlands & TNO – Dutch
12 Geological Survey, Utrecht, The Netherlands, previously at²

13 ⁵Advanced Groundwater Techniques (AGT), Kontich, Belgium

14 ⁶Vivaqua, Brussel, Belgium, previously at University of Liege, Urban and Environmental Engineering,
15 Belgium.

16 ⁷ Lawrence Berkeley National Laboratory, EESA, Berkeley, CA, US

17 Correspondence: Luka Tas <luka.tas@ugent.be>

18

19 **Abstract**

20 *Aquifer Thermal Energy Storage (ATES) has great potential to mitigate CO₂ emissions associated with the*
21 *heating and cooling of buildings and offers wide applicability. Thick productive aquifer layers have been*
22 *targeted first, as these are the most promising areas for ATES. Regardless, there is currently an increasing*
23 *trend to target more complex aquifers such as low-transmissivity and alluvial aquifers or fractured rock*
24 *formations. There, the uncertainty of subsurface characteristics and, with that, the risk of poor-performing*
25 *systems is considerably higher. Commonly applied strategies to decide upon the ATES feasibility and well*
26 *design standards for optimization may need to be adapted. To further promote the use of ATES in such*
27 *less favorable aquifers an efficient and systematic methodology evaluating the optimal conditions, while not*
28 *neglecting uncertainty, is crucial. In this context, the distance-based global sensitivity analysis (DGSA)*
29 *method is tested. The analysis focuses on one promising thick productive aquifer, first used to validate the*
30 *methodology, as well as a complex shallow alluvial aquifer. Through this method, multiple random model*
31 *realizations are generated by sampling each parameter from a predetermined range of uncertainty. The*
32 *DGSA methodology validates that the hydraulic conductivity, the natural hydraulic gradient and the annual*
33 *storage volume dominate the functioning of an ATES system in both hydrogeological settings. The method*
34 *also advances the state of the art in both settings. Darcy flux measurements can provide a first prediction*
35 *of the relative ATES efficiency ahead of investing in more detailed studies. Unsensitive parameters can be*
36 *fixed to average values without compromising on prediction accuracy justifying streamlined models in the*
37 *future. It also demonstrates the insignificance of seasonal soil temperature fluctuations for very shallow*
38 *storage of thermal energy and it clarifies the thermal energy exchange dynamics directly above the storage*
39 *volume in unconfined shallow aquifers. Analysis of the parameter distributions allowed us to gain more*
40 *insights into favorable conditions for ATES and to propose a cut-off criterion for its application in alluvial*
41 *aquifers with high natural hydraulic gradient. The nuanced understanding gained with this study contributes*
42 *to the optimization of ATES systems, offering practical guidance for enhanced efficiency of feasibility*
43 *studies, especially in challenging environments. The broad prior uncertainty strategy proves its value by*
44 *expanding (while clearly delimiting) the applicability of the findings.*

45

**This is a non-peer-reviewed preprint submitted to EarthArXiv.
It is under review in Geothermal Energy.**

46 **Keywords**

47 aquifer thermal energy storage (ATES), sensitivity analysis, uncertainty, shallow aquifers, optimization,

48 stochastic method

49 **1 Introduction**

50 Low-temperature aquifer thermal energy storage (ATES) systems can provide heating and cooling to large
51 buildings in a green and sustainable way saving on average 0.5 kg of CO₂ for every cubic meter of water
52 extracted (Fleuchaus et al., 2018; Ramos-Escudero et al., 2021; Jackson et al., 2024). In essence, during
53 summer excess heat from buildings is stored in the subsurface, ready to be used for heating in winter.
54 Conversely, during winter cold is stored in the subsurface to provide cooling in warmer months.

55 Due to its sustainable nature and wide applicability, the interest in investing in ATES is experiencing
56 significant growth. For example, in Flanders (northern Belgium), the number of operational systems has
57 steadily increased from 30 to 368 over the past five years (Databank Ondergrond Vlaanderen, n.d.). In
58 Wallonia (southern Belgium) and Brussels (central Belgium) this growth manifests differently. There, more
59 complex aquifers, respectively a shallow alluvial (De Schepper et al., 2020) and a fractured aquifer (De
60 Paoli et al., 2023), were targeted for ATES despite the high uncertainty. Meanwhile, the Netherlands
61 continue to take the lead with thousands of operational systems (Jackson et al., 2024). The growing interest
62 has stimulated research in this field to improve understanding of the groundwater and heat transport
63 processes occurring in the aquifer. Studies demonstrated that the thermal recovery efficiency of ATES
64 systems depends on thermal conduction and dispersion, regional groundwater flow, and density-dependent
65 flow (only significant at higher temperatures) (Doughty et al., 1982; Gao et al., 2017; Bloemendal and
66 Olsthoorn, 2018; Bloemendal and Hartog, 2018). Consequently, the porous media heterogeneity, for
67 instance in terms of hydraulic conductivity, can significantly impact thermal energy storage (Ferguson,
68 2007; Bridger and Allen, 2010).

69 Even though ATES already has a widespread implementation, uncertainties in thermal and hydraulic
70 properties persist when aiming to make robust predictions on thermal energy storage and recovery
71 efficiency (Hermans et al., 2019; Heldt et al., 2024; Jackson et al., 2024). This particularly presents
72 challenges when targeting more complex, more unknown (deeper) aquifers where it is insufficient to rely
73 on design standards and experience for decision-making (Winter, 2004; Renard, 2007; Tas et al., 2023).
74 Currently, during the preliminary stage of ATES feasibility studies, a desktop study is carried out and in
75 many cases it becomes apparent that wide ranges of variation are reported for several hydraulic and

76 thermal parameters in databases and literature. To be able to efficiently design an ATEs system it is crucial
77 to have a thorough and systematic method to determine which uncertain parameters influence the recovery
78 of the thermal energy the most. Similarly, when targeting complex settings with more uncertain parameters
79 the potential shift of sensitive parameters needs to be understood. In this way, a field campaign can be
80 designed that targets the sensitive parameters and thus substantially reduces the uncertainty.

81 Besides this, in traditional modelling the values of the uncertain parameters are often chosen based on
82 deterministic calibration or they are set based on experience/expert judgement. This approach overlooks
83 the fact that a calibrated model is non-unique and it fails to acknowledge that substantiated research should
84 precede making model simplifications such as fixing model parameters to average values (Sommer et al.,
85 2013; Farmer and Vogel, 2016; Hoffmann et al., 2019; Hermans et al., 2023). To gain insights into the
86 recoverability of stored thermal energy in a certain geological setting, this prior uncertainty should initially
87 be considered for each parameter. This also creates the opportunity to analyze parameter distributions,
88 potentially identifying favorable conditions for ATEs and vice versa conditions that should be avoided
89 (Renard, 2007; Ferré, 2017).

90 The stochastic approach of a distance-based global sensitivity analysis (DGSA) can tackle these issues
91 (Farmer and Vogel, 2016). It has been proven efficient in determining the model variables having the largest
92 influence on the data and the prediction for hydrogeological applications (Scheidt et al., 2018; Hermans et
93 al., 2019; Hoffmann et al., 2019). The DGSA methodology distinguishes itself because it allows for the
94 models to be sufficiently general in terms of prior uncertainty so that the early conclusions can be
95 generalized and findings widely applied (Farmer and Vogel, 2016).

96 This paper aims to provide an original validation of the versatility and efficiency of the DGSA methodology
97 by applying it to realistic long-term models of ATEs systems in two distinct hydrogeological settings. We
98 will simultaneously include uncertainty on the model parameters, boundary conditions and operational
99 parameters. The first study case focuses on the traditional ATEs target of a thick productive aquifer. Beyond
100 serving to validate the methodology, it will advance the state of the art in the prediction approach of the
101 ATEs efficiency. Specifically, this study will offer a fresh perspective on how the efficiency and prediction
102 accuracy of ATEs systems relate to the choice of the uncertain variables and to the heat transport

103 processes. The second case shifts the focus to a more complex and uncertain ATES target: a shallow
104 alluvial aquifer characterized by a high natural hydraulic gradient. The results will offer novel insights into
105 the influence of diverse heat transport processes on the efficiency of thermal storage in very shallow
106 aquifers. In particular, this framework will be applied to research the influence of seasonal soil temperature
107 fluctuations. This has so far been overlooked, disregarding a potentially significant impact. Overall, the
108 results of the sensitivity analyses will provide a substantiated basis to streamline models in the future. By
109 directly linking the thermal recovery efficiency to the most influential parameters, we aim to identify relations
110 that are key to optimizing feasibility studies and decision-making processes. The broad prior uncertainty
111 strategy, characteristic of the DGSA method and neglected in previous ATES studies, will promote the wide
112 applicability of the findings.

113 **2 Study cases**

114 **2.1 Case 1: thick productive aquifer**

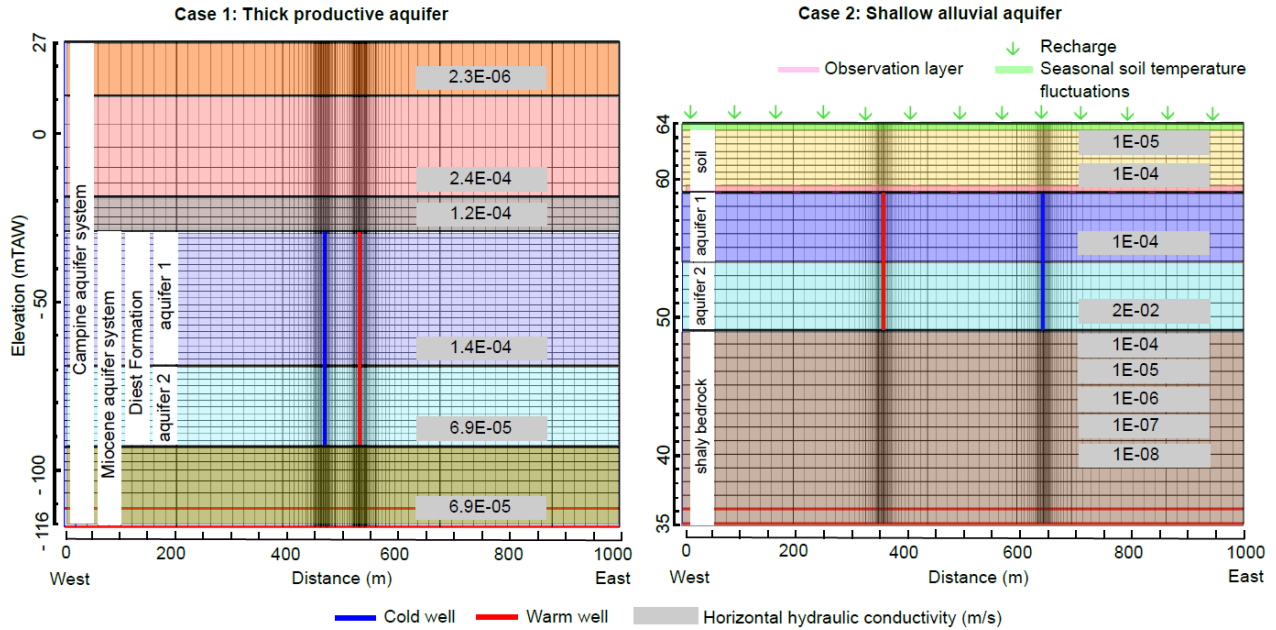
115 As a first case a thick sandy aquifer, capable of sustaining high flow rates, is selected. Due to its suitability,
116 many operational ATES systems have been installed in this kind of aquifer. Therefore, from experience and
117 literature, there is a thorough understanding of the groundwater flow and heat transport processes in these
118 prevalent settings. This prior knowledge allows us to test the methodology of DGSA for ATES and to
119 evaluate the output with discernment.

120 The studied case represents an operational ATES system in Rijkevorsel, Belgium. The wells are screened
121 in the sandy Diest Formation which extends from -29 mTAW (meters above average sea level at low tide)
122 to -93 mTAW and is part of the Miocene aquifer system (Fig. 1). The upper part of this formation has a
123 thickness of 40 m and typically has a higher hydraulic conductivity than the lower part. Above the screened
124 interval sandy to clayey-sandy formations are present. Below the screened interval the sandy Berchem
125 and/or Voort Formation is present up to -116.5 mTAW, bounded below by the Boom aquitard. Even though
126 the case is based on a specific location, the findings of the study have broad applicability across various
127 areas because of varying model parameters and boundary conditions in the analysis (see 3.4).

128 **2.2 Case 2: shallow alluvial aquifer**

129 Second, an alluvial aquifer was chosen. It is typically characterized by a high hydraulic conductivity and
130 thus also constitutes a good target for ATEs when the ambient groundwater flow is slow, as shown by De
131 Schepper et al. (2019) and Fossoul et al. (2011). Though, the occurrence of clay lenses can locally cause
132 lower productivity (Fossoul et al., 2011; Robert et al., 2018). A main concern however is a potential loss of
133 stored thermal energy towards the atmosphere because of the shallow nature of the aquifer. This case
134 aims to provide an improved understanding of the heat transport processes between the ground surface,
135 which is subject to seasonal soil temperature fluctuations, and the shallow aquifer used for storage. It will
136 also provide new insights into the suitability of shallow alluvial aquifers for ATEs by relating the efficiency
137 to design parameters, boundary conditions and model parameters.

138 The studied case is representative of the alluvial aquifer of the Meuse River in the region of Liege (Wallonia,
139 Belgium) but can represent various shallow alluvial aquifer scenarios (see 3.4). There is currently one
140 operating ATEs system in this aquifer (De Schepper et al., 2020) and the area is highly investigated with
141 field tests (Fossoul et al., 2011; Battle-Aguilar et al., 2009; Wildemeersch et al., 2014; Klepikova et al.,
142 2016; De Schepper et al., 2019; Hermans et al., 2019). Therefore there is a good estimation of the (heat)
143 transport parameters and the hydrogeology. Below the ground surface, heterogeneous soil sediments and
144 backfill are present. The aquifer in which the wells are screened is located from +59 mTAW to +49 mTAW
145 and can be divided into two layers of equal thickness (Fig. 1). The upper aquifer layer is composed of sandy
146 gravels and the lower aquifer layer is composed of coarse clean gravels. The aquifer is bounded below by
147 shaly bedrock with a decreasing degree of weathering downwards. Important to note is that lateral
148 heterogeneity plays an important role in alluvial aquifers (Klepikova et al., 2016), however, the influence of
149 this has already been thoroughly analyzed with a sensitivity analysis by Hermans et al. (2019) and is for
150 simplicity omitted for this study.



151

Fig. 1. Hydrogeological representation of the two studied cases with an indication of the calibrated horizontal hydraulic conductivity values (in m/s).

152 3 Methods

153 3.1 Heat transport processes in the shallow subsurface

154 In the alluvial aquifer, thermal energy storage happens very shallow and the influence of the air temperature
 155 cannot be excluded. During winter the warm storage area typically has a higher temperature than the air,
 156 leading to a potential energy loss towards the surface. Similarly, the cold storage area may experience
 157 energy gain. During summer this effect may be reversed. Even though this phenomenon is of significant
 158 interest for understanding the thermal recovery efficiency of ATEs systems in shallow aquifers, it has not
 159 yet been investigated. Nonetheless, heat losses in ATEs systems have been thoroughly investigated. The
 160 main drivers in low-temperature ATEs are conduction and dispersion occurring at the surface area (A)
 161 between the volume of stored heated groundwater and the ambient groundwater (Doughty et al., 1982;
 162 Bloemendal and Hartog, 2018; Beernink et al., 2024). Generally, for the traditional range of storage
 163 conditions of ATEs systems in the Netherlands, losses by conduction dominate over those by dispersion.
 164 Therefore, a fundamental parameter in analyzing these losses is the storage volume (V), which must be as
 165 compact as possible (i.e. minimize A/V) to minimize heat losses. Next, it has also been demonstrated that
 166 dispersion losses are negligible through the upper and lower surfaces of confined aquifers (Beernink et al.,

167 2024). However, case 2 does not represent a fully confined aquifer and a vertical flux through the soil layers
168 above the aquifer must be considered. This flux can result from the ATEs well operations and from the
169 recharge that is applied on the top of the aquifer (Fig. 1).

170 We strived to represent the thermal energy exchange between the storage aquifer and the atmosphere by
171 imposing a sine-shaped soil temperature profile with a monthly time discretization on top of the model (Fig.
172 1). Soil temperature rather than air temperature was selected as it is the surface temperature that drives
173 the shallow subsurface thermal regime (Kurylyk et al., 2015). The variations in soil temperature will be
174 strongly attenuated downwards in the ground because of the high heat capacity of water and the lag of the
175 surface temperature effect also increases downward. Already at depths of more than a few meters, the
176 variations in the top soil are negligible, which justifies why this temperature variation is typically neglected
177 when deeper geothermal systems are modelled (Claesson and Eskilson, 1988; Preene and Powrie, 2009;
178 Kurylyk et al., 2015).

179 Note that even though the alluvial aquifer is not fully confined, it was modelled as a confined aquifer to allow
180 setting a fine vertical grid discretization accurately modelling the heat transport processes. As a result, the
181 aquifer was modelled as fully saturated when in reality the groundwater table is found 3 m below the surface.
182 This choice remains valid for the purpose of the study considering the prior uncertainty range of the top
183 temperature and it can serve as a worst-case scenario as the unsaturated layer would act as an insulator.

184 **3.2 Modelling Approach**

185 *3.2.1 Software*

186 For this project, the freely available USGS MODFLOW 2005 software (v1.12.00) was used to simulate
187 groundwater flow (Harbaugh et al., 2017). To model the (heat) transport processes, MT3D-USGS was used
188 (Bedekar et al., 2016), taking advantage of the analogy between the heat transport and solute transport
189 equations as previously shown and validated (Hecht-Méndez et al., 2010; Ma and Zheng, 2010; Fossoul et
190 al., 2011; Sommer et al., 2013; Tas et al., 2023). Water density was considered constant which is a fair
191 assumption when the temperature changes remain limited for a low-temperature ATEs system ($\Delta T < 15^\circ\text{C}$)
192 (Zuurbier et al., 2013; Zeghici et al., 2015). To set up the model, ModelMuse version 5.1.1 was used as a
193 graphical user interface (Winston, 2022). To be able to run many MODFLOW-based models with different

194 parameters efficiently for the sensitivity analysis, the Python package FloPy was used (Bakker et al., 2016;
195 Hughes et al., 2024). Details on the influence of grid discretization and boundary conditions on the
196 prediction as well as details on the influence of the solver settings on numerical dispersion can be consulted
197 in the supplementary material (S1, S2).

198 *3.2.2 Computational demand*

199 To overcome the substantial computational demand of running multiple simulations (see section 3.3), the
200 supercomputing facilities of Ghent University were used. The workload could be viewed as embarrassingly
201 parallel assigning each simulation to a single CPU. Performing the tasks in this way resulted in a maximum
202 computational requirement of ~ 72 hours and ~ 8 Tib of short-term storage per case.

203 **3.3 Distance-based global sensitivity analysis**

204 A sensitivity analysis provides information on the leverage of each input variable to the output and can
205 therefore be of great interest during feasibility studies and decision-making processes. The knowledge of
206 high-influential parameters can be used to determine which field data needs to be acquired to reduce the
207 uncertainty. Furthermore, SA can reduce model complexity by fixing low-influential parameters and it can
208 advance our understanding of the modeled system by analyzing the model response to parameter variation
209 (Lu and Ricciuto, 2020).

210 In previous sensitivity studies of ATEs systems often tens of distinct model realizations were chosen to
211 draw conclusions with a structured SA (Schout et al., 2014; Poulsen et al., 2015; Bloemendal and Hartog,
212 2018; Beernink et al., 2024; Heldt et al., 2024) or a methodology was used that requires a computationally
213 impractical amount of runs to be accurate. For instance, Sobol's method, which is a form of GSA based on
214 variation decomposition, is frequently employed (Jeon et al., 2015; Lu and Ricciuto, 2020; Stemmler et al.,
215 2021) but it may miss-predict the sensitivity value due to complex dependence among variables (Hoteit et
216 al., 2023).

217 The distance-based global sensitivity analysis (DGSA) has been proven a computationally efficient and
218 statistically significant method by relying on a clustering of the model response (Scheidt et al., 2018;
219 Hermans et al., 2019; Lu and Ricciuto, 2020) and its applicability for ATEs systems will be validated in this

220 paper. Essentially, the DGSA consists of first sampling model realizations from the predefined ranges of
221 uncertainty for each parameter (i.e. the prior distribution) and generating the model output. For cases 1 and
222 2, 250 and 500 model realizations were sampled respectively (the number of realizations was obtained by
223 trial and error) (Zhang et al., 2024). In this study, the output is the temperature evolution at the warm and
224 cold ATES wells over time, recorded every 0.5 days and, in the case of the alluvial aquifer, also the energy
225 exchange with the atmosphere. Next, the model output is classified (KMedoids/KMeans) into an appropriate
226 number of clusters, which can be verified by the Davies-Bouldin index and the mean silhouette index
227 (Davies and Bouldin, 1979; Kaufman and Rousseuw, 1990; Scheidt et al., 2018). When the cluster
228 cumulative distribution functions (cdf) of a certain parameter significantly differ, the parameter is deemed
229 sensitive (Fenwick et al., 2014; Scheidt et al., 2018; Lu and Ricciuto, 2020).

230 With this method, the standardized class-conditional sensitivity for each parameter but also the mean
231 sensitivity averaged over all classes, can be determined. Similarly, the sensitivity of parameter interactions
232 can be determined based on their conditional distributions. The application of the DGSA method was
233 facilitated by the user-friendly pyDGSA Python package (Fenwick et al., 2014; Park et al., 2016).

234 **3.4 The prior distribution of the cases**

235 For this study, the model realizations are sampled randomly from a uniform distribution with the Latin
236 hypercube sampling method to ensure a well-distributed coverage across the sample space (Heldt et al.,
237 2024). The ensemble of all possible model realizations is called the prior distribution.

238 For case 1, the horizontal and vertical hydraulic conductivity, the total and effective porosity, the ambient
239 groundwater flow (prescribed hydraulic gradient) and the longitudinal dispersion were varied. In case 2, the
240 temperature of the soil (top boundary condition), the recharge and the annual storage volume were
241 additionally varied. Only for the hydraulic conductivity a distinction was made between the upper and lower
242 parts of the aquifers. As the natural variability in thermal properties is orders of magnitude less than the
243 natural variability in hydraulic properties more homogeneous assumptions for heat transport are justified
244 (Kurylyk et al., 2015). The detailed ranges of variation for both cases can be consulted in Table 1 and Table
245 2 and a clarification on the choice of the lower and upper limits is provided in the supplementary materials
246 (S3).

247 The vertical hydraulic conductivity was determined as a ratio from the horizontal hydraulic conductivity with
248 K_h/K_v ratios varying from 2 to 10. Similarly, the effective porosity was calculated as a percentage of the
249 total porosity, ranging from 50 to 80%. The horizontal and vertical transversal dispersion were set at 1/10
250 and 1/100 of the longitudinal dispersion, respectively.

251 **Table 1:** Parameter values and prior definition of the thick productive aquifer. For the parameters in bold, a random
252 value within the range of variation was selected for the model realizations of the DGSA.

Parameter	Unit	Initial value		Range of variation	Package
<i>Hydrogeological parameters</i>					
Horizontal hydraulic conductivity (K_h)	m/s	<i>Aqf 1</i>	1.39E-04	U[1.00E-04 - 6.00E-04]	LPF
		<i>Aqf 2</i>	6.954E-05	U[5.00E-05 - 2.00E-04]	
Vertical hydraulic conductivity (K_v)	m/s	<i>Aqf 1</i>	4.63E-05	U[1.00E-05 - 3.00E-04]	LPF
		<i>Aqf 2</i>	2.31E-05	U[5.00E-06 - 1.00E-04]	
Total porosity ($n_{Tot. por.}$)	-	0.35		U[0.25 - 0.5]	RCT, DSP
Effective porosity ($n_{Eff. Por.}$) ~ specific yield (S_y)	-	0.3		U[0.125 - 0.4]	BTN, LPF
Specific storage	m^{-1}	0.0001		-	LPF
Longitudinal dispersivity ($\alpha/Long. disp$)	m	1		U[0.5 - 5]	DSP
Initial temperature (T_0)	$^{\circ}C$	12		-	SSM, BTN
Density water (ρ_w)	kg/m ³	1000		-	-
Density solid (ρ_s)	kg/m ³	2650		-	-
Bulk density (ρ_b)	kg/m ³	$\rho_s \times (1 - nt)$		U[1325 - 1988]	RCT
Thermal conductivity water (kw)	W/(m ² C)	0.58		-	-
Thermal conductivity solid (ks)	W/(m ² C)	2.4		-	-
Bulk thermal conductivity (kb)	W/(m ² C)	$kw \times nt + ks \times (1 - nt)$		[1.49 - 1.945]	-
Specific heat capacity solid (cs)	J/(kg ² C)	730		-	-
Specific heat capacity water (cw)	J/(kg ² C)	4183		-	-
Thermal distribution coefficient (K_d)	m ³ /kg	$cs/(cw \times \rho_w)$		-	RCT
Effective molecular diffusion coefficient (Dm)	m ² /s	$kb \div (nt \times \rho_w \times cw)$		U[7.12E-07 - 1.86E-06]	DSP
<i>Boundary conditions</i>					
Prescribed hydraulic gradient ($Grad.$)	%	0.1		U[0 - 0.3]	CHD
<i>Design parameters</i>					
Injection and extraction rate (Q)	m ³ /s	2E-3 to 1E-4 (see scenario Table 3)		-	WEL
Injection temperature, relative to T_0 (ΔTin_j)	$^{\circ}C$	+/- 5 (see scenario Table 3)		-	SSM

254 **Table 2:** Parameter values and prior definition of the shallow alluvial aquifer. For the parameters in bold, a random
255 value within the range of variation was selected for the model realizations of the DGSA.

Parameter	Unit	Initial value		Range of variation	Package
<i>Hydrogeological parameters</i>					
Horizontal hydraulic conductivity (K_h)	m/s	<i>Aqf 1</i>	1.00E-04	U[1.00E-05-1.00E-03]	LPF
		<i>Aqf 2</i>	2.00E-02	U[1.00E-03-1.00E-01]	
Vertical hydraulic conductivity (K_v)	m/s	<i>Aqf 1</i>	1.00E-05	U[1.00E-06-5.00E-04]	LPF
		<i>Aqf 2</i>	2.00E-03	U[1.00E-04-5.00E-02]	
Total porosity (n_t/Tot. por.)	-			U[0.25 - 0.5]	RCT, DSP
Effective porosity (n_e/Eff. por.) ~ specific yield (S_y)	-	0.3		U[0.125 - 0.4]	BTN, LPF
Specific storage	m ⁻¹	5.00E-02		-	LPF
Longitudinal dispersivity (α_l/Long. disp.)	m	5		U[0.5 - 5]	DSP
Initial temperature (T_0)	°C	Average of T_s		-	SSM, BTN
Density water (ρ_w)	kg/m ³	1000		-	-
Density solid (ρ_s)	kg/m ³	2650		-	-
Bulk density (ρ_b)	kg/m ³	$\rho_s \times (1 - nt)$		U[1325 - 1988]	RCT
Thermal conductivity water (k_w)	W/(m°C)	0.58		-	-
Thermal conductivity solid (k_s)	W/(m°C)	3		-	-
Bulk thermal conductivity (k_b)	W/(m°C)	$k_w \times nt + k_s \times (1 - nt)$		[1.79 – 2.395]	-
Specific heat capacity solid (c_s)	J/(kg°C)	878		-	-
Specific heat capacity water (c_w)	J/(kg°C)	4183		-	-
Thermal distribution coefficient (K_d)	m ³ /kg	$c_s / (c_w \times \rho_w)$		-	RCT
Effective molecular diffusion coefficient (D_m)	m ² /s	$k_b \div (nt \times \rho_w \times c_w)$		U[8.56E-07- 2.29E-06]	DSP
<i>Boundary conditions</i>					
Prescribed hydraulic gradient (Grad.)	%	0.1		U[0 – 0.2]	CHD
Recharge	m/s	2.00E-09		U[5.29E-09 -8.46E-09]	RCH
Soil temperature (T_s)	°C	Winter (T_{winter})	4	U[2.5-8]	SSM
		Summer (T_{zomer}) (May-October)	16	U[15-20.5]	
<i>Design parameters</i>					
Annual storage volume (V)	m ³	200000		U[12500-200000]	WEL
Injection temperature, relative to T_0 (ΔT_{inj})	°C	5		-	SSM

256

257 **3.5 Assessment Framework**

258 **3.5.1 Modelling scenarios**

259 The model of case 1 mimics, in terms of flow rate and injection temperature, the functioning of the
260 operational ATES system. The choice was made to use the first 7 months of monitoring data, repeated 3
261 times, for the DGSA. The monitoring data was considered with a monthly time discretization (half-monthly
262 for October) and simplifications were made because, in reality, the ATES system could quickly switch
263 between heating and cooling modes when it was required. Mimicking the operational system means that
264 the storage volume in cooling mode did not equal the storage volume in heating mode (Table 3).

265 **Table 3:** Scenario for the DGSA of the ATES system in the thick productive aquifer based on monitoring data available
266 from the operational system in Rijkvorseel. This scenario is repeated 3 times to represent 3 full operational cycles.

Stress period (-) - duration (days)	Flowrate cold well (m3/s)	Flowrate warm well (m3/s)	Injection temperature warm well (°C)	Injection temperature cold well (°C)
1 - 31	-0.002329	0.002329	14.34	-
2 - 31	-0.001254	0.001254	14.61	-
3 - 30	-0.000136	0.000136	16.92	-
4 - 11	-0.000200	0.000200	14.33	-
5 - 20	0.000323	-0.000323	-	9.01
6 - 30	0.000451	-0.000451	-	8.49
7 - 31	0.000552	-0.000552	-	7.76
8 - 31	0.000948	-0.000948	-	7.20

267

268 For case 2, a two-year simulation was used starting with the cooling season (typically the first of May). Heat
269 was stored during the initial 180 days of each year and cold was stored during the subsequent 180 days,
270 employing a synthetic sine-shape profile with a monthly time discretization for the flow rate of the system.
271 This means that the injected volume equals the extracted volume.

272 3.5.2 Thermal Recovery Efficiency

273 Once the sensitive parameters were determined, their values were associated with the thermal recovery
274 efficiency of the ATES system. This is often used as the main indicator of the overall energy savings of
275 ATES systems and it is both affected by storage specifics and site-specific hydrogeological conditions
276 (Bloemendal and Hartog, 2018). The thermal recovery efficiency can be calculated for each season as the
277 percentage of thermal energy that can be extracted from the energy that was stored in the previous cycle
278 (Duijff et al., 2021; Tas et al., 2023; Beernink et al., 2024):

$$279 \eta_{th} = \frac{E_{ex}}{E_{in}} = \frac{\int_0^t Q_{ex} c_w \Delta T dt}{\int_0^t Q_{in} c_w \Delta T dt}$$

280 where E_{ex} and E_{in} (kWh) are the extracted and injected energy, Q_{ex} and Q_{in} (m^3/h) the total extraction and
281 injection flow rate of the system, c_w the specific heat capacity of water (1.16 kWh/ m^3K), ΔT ($^{\circ}C$) is the
282 absolute temperature difference between the injected/extracted water and the ambient groundwater
283 temperature of the aquifer, and t (h) is time.

284 3.5.3 Thermal energy exchange

285 To explore the influence of seasonal soil temperature fluctuations on the efficiency of shallow ATES
286 systems, the thermal energy exchange between the storage aquifer and the soil was determined.
287 Conceptually, the soil layer of 0.5 m thickness, right above the aquifer, was used as an observation layer
288 (Fig. 1). In every cell of this layer, the vertical mass flux Q_v (m^3/h) and the absolute temperature difference
289 between the temperature of each cell and the ambient groundwater temperature ΔT_{abs} ($^{\circ}C$) were analyzed
290 to derive the energy exchange (Exchange, kWh) per season:

$$291 E_{exchange} = \int_0^t Q_v c_w \Delta T_{abs} dt$$

292 When the energy exchange is calculated for each cell, the total energy exchange through the entire layer
293 or the areas right above cold and warm thermal energy storage can be determined. Subsequently, a DGSA
294 can be done based on the energy exchange per season and the influential parameters can be associated
295 with the thermal energy exchange or the thermal recovery efficiency. The necessity of applying sine-shaped

296 temperature profiles reflecting the shallow soil temperature variations in alluvial aquifers for ATES was also
297 assessed. This was accomplished by comparing the energy exchange results to the output of models where
298 the top boundary condition had a constant temperature, equal to the natural average groundwater
299 temperature.

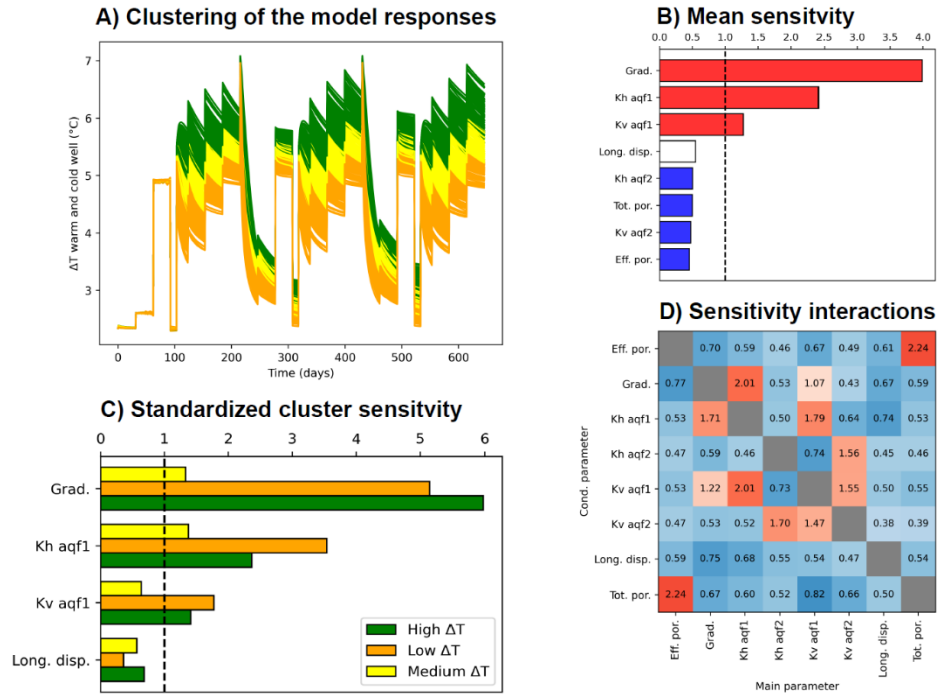
300 **4 Results**

301 **4.1 Case 1: Thick productive aquifer**

302 *4.1.1 Parameters sensitive to the temperature evolution over time*

303 The temperature difference between both wells is used for the DGSA. To determine the sensitive
304 parameters, first, the model responses were clustered into three classes (Fig. 2A). The KMedoids clustering
305 method was used and it was confirmed that the KMeans method does not yield a different outcome. The
306 derived classes represent model realizations exhibiting generally high/medium/low temperature differences,
307 corresponding to field conditions which lead to the most/less/least efficient ATES systems in this type of
308 study area.

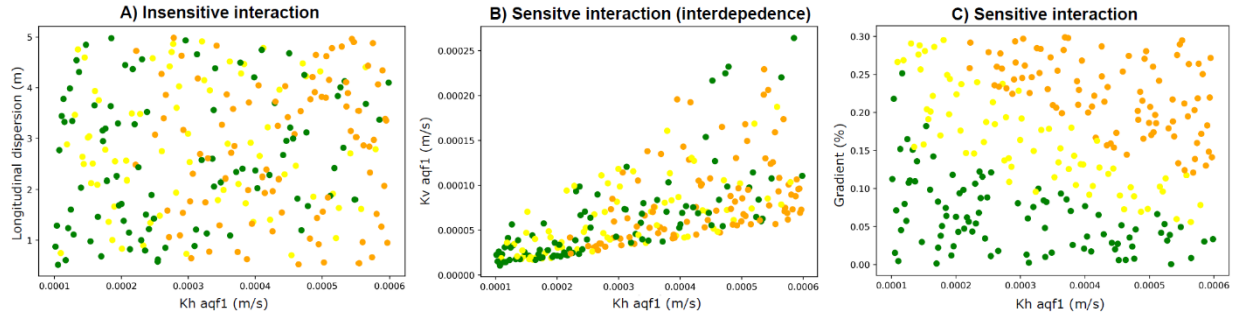
309 The mean sensitivity reveals that the natural hydraulic gradient and the vertical and horizontal hydraulic
310 conductivity of the upper aquifer layer are the sensitive parameters (Fig. 2B, 2C). The conductivity of the
311 lower aquifer layer is not sensitive. This aligns with our expectations because the lower aquifer contributes
312 less to the total flow rate of the ATES system.



313

Fig. 2. DGSA results of case 1. A) The temperature evolution with time in the thick productive aquifer clustered into 3 classes, B) the mean standardized sensitivity for all parameters, C) the cluster standardized sensitivity of the top 4 influential parameters, D) the standardized sensitivity of interactions between parameters.

314 Nevertheless, if an insensitive parameter contributes to a sensitive interaction with another parameter, it
 315 should still be considered for further analysis. The interaction matrix in Fig. 2D highlights interactions
 316 between the total and effective porosity and between horizontal and vertical hydraulic conductivity for both
 317 aquifer layers which were not further explored as these are parameters that were linked to each other in
 318 the prior (Table 1). This is also visible in Fig. 3B as the parameter distribution does not expand across the
 319 entire 2D parameter space. Next to this, also interactions between the gradient and the hydraulic
 320 conductivity of the upper aquifer layer become apparent. Plotting the parameter distribution of these two
 321 variables against each other reveals a distinct boundary between the classes (Fig. 3C). If the interaction
 322 between two parameters is insensitive, clusters are mixed (Fig. 3A).



323

Fig. 3. Parameter distribution clarifying the type of parameter interactions ranging from insensitive (A), to apparently sensitive (B) and truly sensitive (C) interactions. The model realizations are colored according to their respective cluster: green, yellow, orange for the high, medium, low efficiency clusters.

324

Fig. 4 gives more insights into the sensitive parameter distribution within the classes. It confirms that ATES

325

systems in study areas characterized by a high natural gradient and a high hydraulic conductivity in the

326

main production layer are the least efficient (Fig. 4A, 4B). This combination facilitates the movement of

327

stored volume away from the extraction area due to the natural groundwater flow, reducing the system's

328

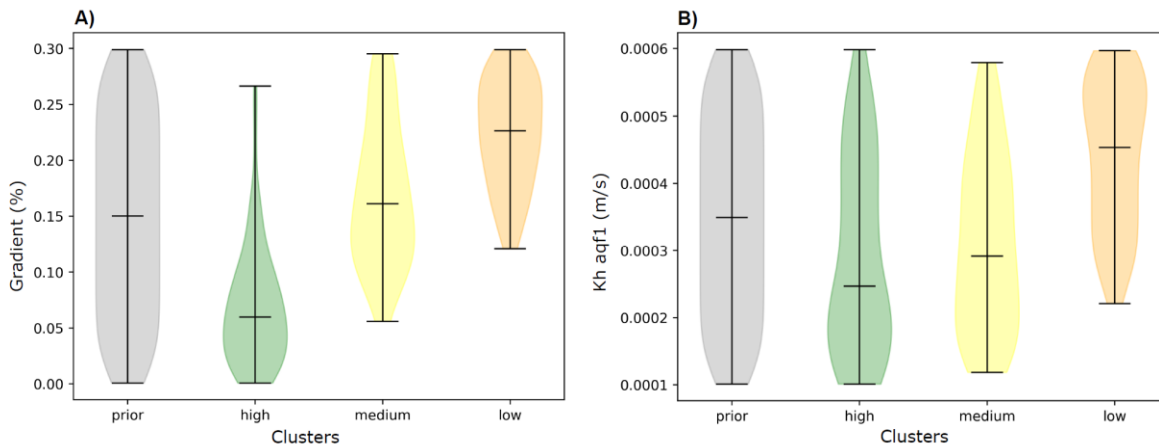
effectiveness. Nevertheless, Fig. 4 also illustrates an overlap of cluster ranges meaning that knowledge of

329

these individual parameters is not sufficient to reduce the uncertainty on the energy efficiency of the ATES

330

system, but that both must be considered together.



331

Fig. 4. Parameter distribution of the prior and the classes of case 1 for A) the natural hydraulic gradient and B) the horizontal hydraulic conductivity of aquifer 1.

332

4.1.2 Thermal recovery efficiency

333

To narrow down the conditions for optimal recovery, we aimed to link the thermal recovery efficiency of the

334

ATES system to the sensitive parameters.

335 The thermal recovery efficiency was calculated for each season. As the efficiency of ATEs systems
336 increases with time, especially in the first seasons, the last season of extraction was selected for
337 comparison with the natural hydraulic gradient, the horizontal hydraulic conductivity and the Darcy flux (Fig.
338 5). Fig. 5A illustrates that when a single sensitive parameter is considered there is a broad spreading or a
339 high uncertainty regarding the efficiency, as Fig. 4 also indicated. This is opposed to Fig. 5B where the
340 Darcy flux, a combination of the two sensitive parameters, exhibits a distinct link with the thermal recovery
341 efficiency. Fig. 5B also shows that there is a significant difference in thermal recovery efficiency between
342 the warm and cold wells for case 1. This owes to the total flow rate of the system which is significantly lower
343 in winter season than in summer season. Apart from this, the results of the sensitive aquifer 1 show that
344 the distinctions between the low and medium and medium and high classes correspond to a Darcy flux of
345 20.5 m/y and 9.5 m/y respectively, for both the warm and the cold well.

346 When the same procedure is applied to the insensitive aquifer 2, the limits do not correspond to the class
347 boundaries anymore (Fig. 5B). This might be attributed to the fact that only the sensitive parameters
348 facilitate the clustering of the model response because only these parameters influence the model response
349 significantly. Therefore using the same clusters and limits to insensitive parameters may not produce
350 meaningful results.

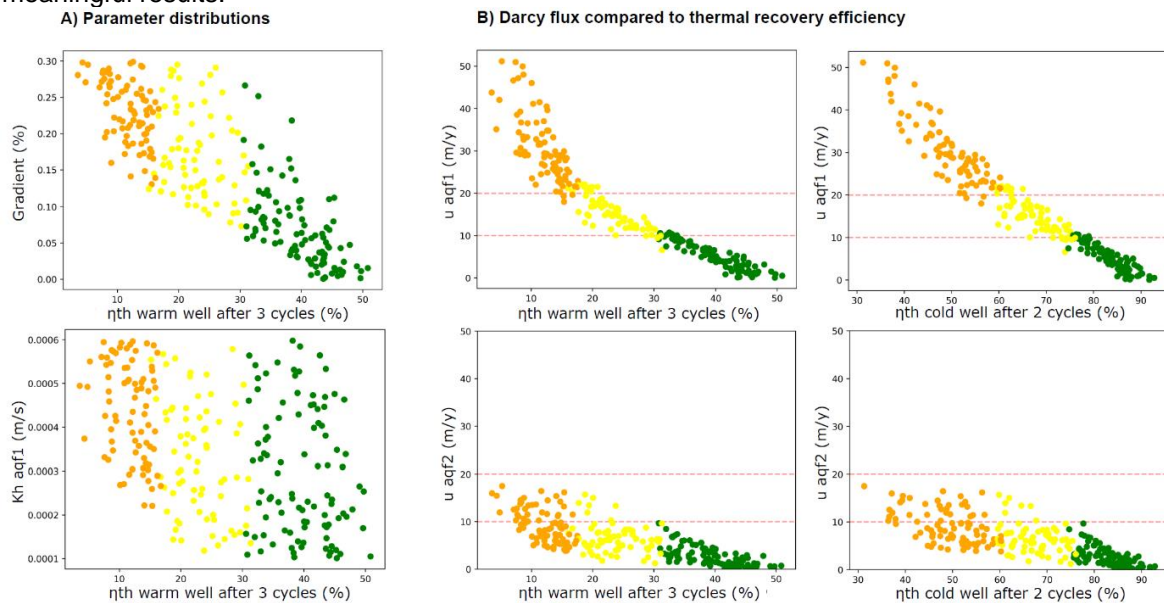


Fig. 5. A) Parameter distributions of the horizontal hydraulic conductivity and the natural gradient showing a general trend but a broad uncertainty (spreading) on the thermal recovery efficiency. B) Illustration of the link between the Darcy flux (u) and the thermal recovery efficiency in case 1 for both the warm and cold well in aquifer 1 and aquifer 2. Model realizations are colored according to their respective cluster.

351 **4.2 Case 2: Shallow alluvial aquifer**

352 **4.2.1 Parameters sensitive to the temperature evolution over time**

353 The clustering of the model responses resulted in two classes, distinguishing between a generally high and
354 low temperature difference, which represent field and/or operational conditions leading to the most and
355 least efficient ATEs systems. They had significantly different sizes, with approximately 420 and 80 samples,
356 necessitating the double amount of samples to obtain statistically significant results (Fig. 6A).

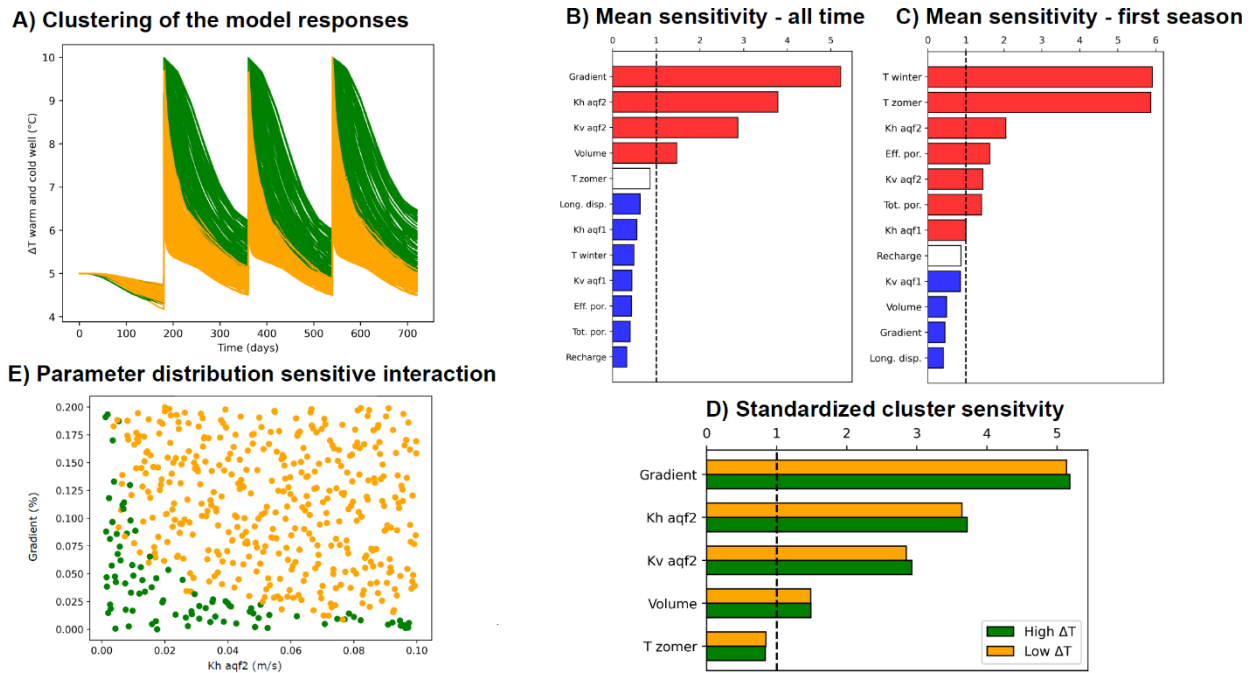
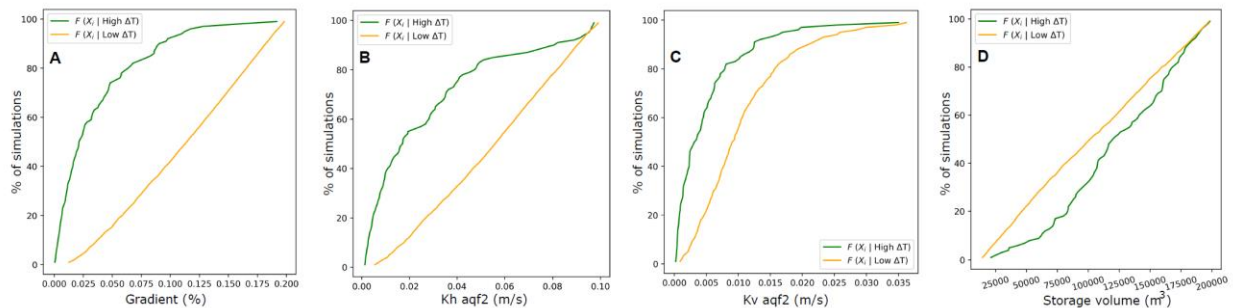


Fig. 6. DGSA results of the temperature evolution with time of case 2. A) Clustering of the model response into two classes, B) mean standardized sensitivity of the full model response for all parameters, C) mean standardized sensitivity of the first season of the model response for all parameters, D) cluster standardized sensitivity of the top 5 influential parameters, E) parameter distribution of the sensitive interaction between the gradient and the horizontal hydraulic conductivity of aquifer 2.

357 The gradient and the vertical and horizontal conductivity of the most transmissive aquifer layer also emerge
358 as the most important parameters influencing the temperature evolution over time. Additionally, the annual
359 storage volume was identified as a sensitive parameter highlighting the significant role of this operational
360 parameter in the system performance (Fig. 6B, 6D). Interestingly, the clustering for the three last seasons
361 yielded desirable results while no clear distinction between classes is observed in the first season (Fig. 6A).
362 This is because the first season only represented injection at a constant temperature and extraction of
363 groundwater at its natural temperature, influenced by the soil temperature in summer season. The following

364 seasons represent the actual recovery of stored thermal energy as is the case for an operating ATES
365 system. To acknowledge this difference a separate DGSA was carried out for the first season which indeed
366 showed that, initially, the top boundary condition has the most significant influence on the model responses
367 (Fig. 6C). Also, the total and effective porosity and the hydraulic conductivity of aquifer 2 are sensitive
368 parameters for the first season demonstrating their importance for heat transport in the shallow subsurface.
369 The interactions between the parameters remained consistent with those of case 1 (Fig. 6E) and the cdf's
370 in Fig. 7 also confirm that generally a low natural gradient and high hydraulic conductivity lead to more
371 efficient systems. The cdf's also reveal that model realizations with larger annual storage volumes retain
372 higher temperature differences (Fig. 7D).

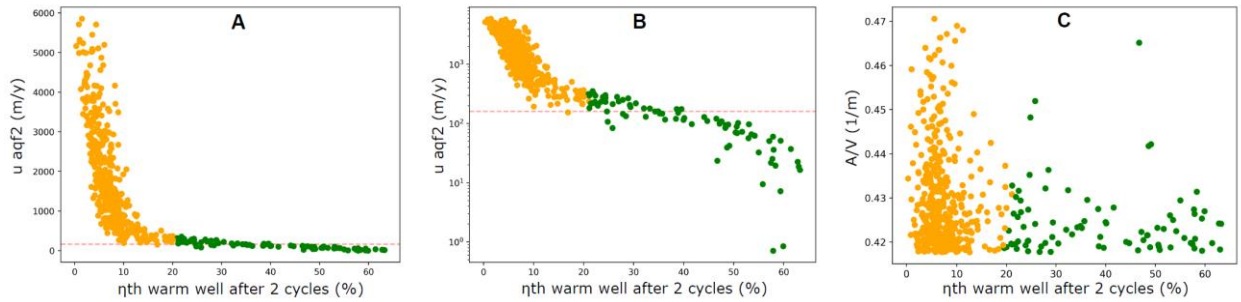


373

Fig. 7. Cumulative distribution functions (cdf's) of case 2 for A) the natural hydraulic gradient, B) the horizontal and vertical conductivity of aquifer 2, and C) the annual storage volume. The model realizations are colored according to their respective cluster: green, and orange for the high and low efficiency clusters.

374 4.2.2 Thermal recovery efficiency

375 Fig. 8 links the thermal recovery efficiency of the ATES system under different field and operational
376 conditions to the Darcy flux. A Darcy flux of approximately 160 m/y is the demarcation (Fig. 8A, 8B) between
377 both classes. Even though the storage volume was identified as sensitive to the temperature evolution over
378 time in the alluvial aquifer, no useful relationship could be derived when comparing the A/V ratio to the
379 thermal energy recovery (Fig. 8C).



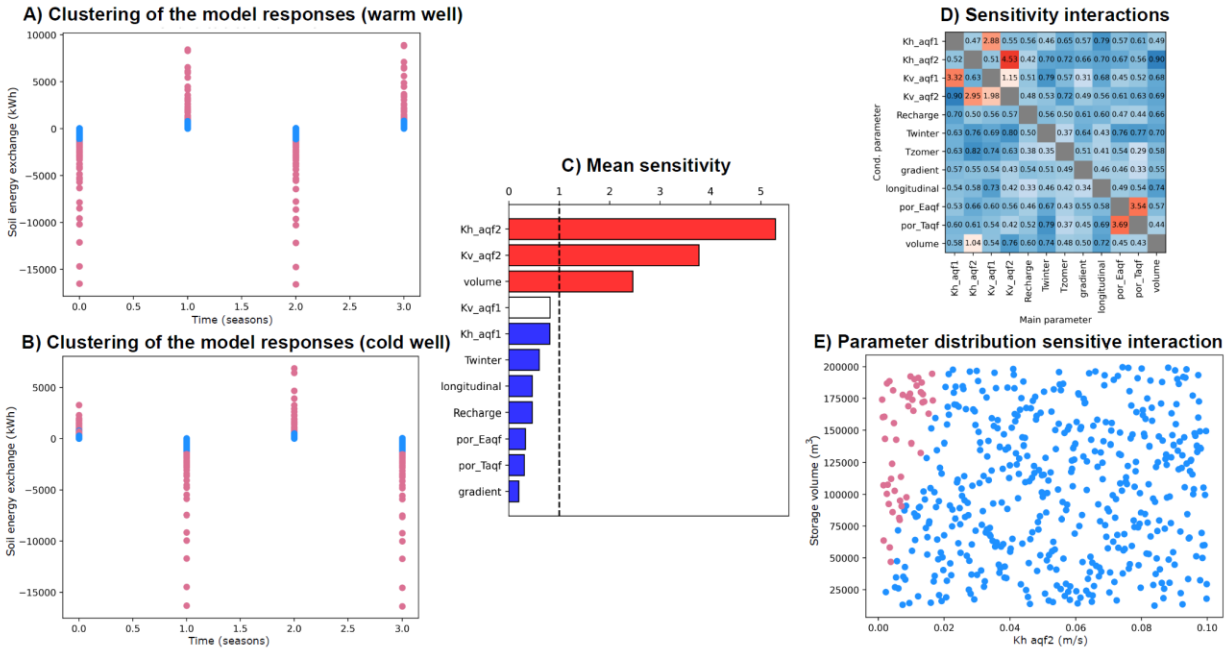
380

Fig. 8. Illustration of the link between the Darcy flux and the thermal recovery efficiency in aquifer 2 of case 2 on a linear (A) and logarithmic scale (B). C) Plot of the thermal recovery efficiency in function of the A/V-ratio. Model realizations are colored according to their respective cluster.

381 4.2.3 Parameters sensitive to the thermal energy exchange

382 An additional DGSA was carried out on the total energy exchange within a small area of 20m by 20m above
383 the warm and cold wells separately, offering perspectives on the dynamics directly above the storage area.
384 Negative values denote an energy gain for the storage area, whereas positive values indicate a loss. This
385 model response was clustered into two classes, the high class corresponding to higher energy gains/losses
386 and the low class corresponding to lower energy gains/losses (Fig. 9A, 9B). The sample distribution across
387 the two classes differs from the classification based on the temperature evolution over time (4.2.1).

388 The conductivity values of the most transmissive aquifer layer are again sensitive parameters as well as
389 the annual storage volume (Fig. 9C). Additionally, there is a sensitive interaction between the horizontal
390 hydraulic conductivity of aquifer 2 and the volume (Fig. 9D). This is reflected in the parameter distribution
391 in Fig. 9E revealing that model realizations with a lower conductivity of aquifer 2 and a high storage volume
392 have significantly higher losses/gains. This might be explained by an increased vertical flow in the
393 neighbourhood of the wells. The natural gradient was no longer identified as a sensitive parameter, which
394 aligns with the expectations when analyzing a small area around the wells. The DGSA of the model
395 realizations with a constant soil temperature equal to the initial temperature of the aquifer show the same
396 results which confirms that the soil temperature is not a sensitive parameter for the energy exchange above
397 the storage area of the ATEs wells.



398

Fig. 9. DGSA results of the thermal energy exchange (20 m by 20 m around wells) in each season of case 2. Clustering of the model response in the warm (A) and cold well (B). C) Mean standardized sensitivity of all parameters, D) sensitivity of the interactions, and E) parameter distribution of the sensitive interaction between the annual storage volume and the horizontal hydraulic conductivity of aquifer 2.

399 *4.2.4 Influence of seasonal soil temperature fluctuations on shallow ATEs*

400 Fig. 9A and 9B show that there are not only losses of energy towards the overlying layer but also gains. It
 401 also reveals that, for shallow aquifers, this energy exchange is not dependent on seasonal soil temperature
 402 fluctuations but it is dominated by the cyclic functioning of the ATEs system itself (Fig. 9C). The amount of
 403 energy exchange is also negligible in comparison to the power produced by the ATEs system (which is
 404 maximum 800 000 kWh for the model realizations) and this insignificance is further confirmed by the fact
 405 that vertical heat losses in one season are counterbalanced by gains in the following season. This means
 406 that also for shallow alluvial aquifers, not overlain by an aquitard, the vertical heat losses are negligible
 407 compared to the lateral losses within the storage aquifer itself.

408 To determine whether it is worth applying a detailed sine-shape profile reflecting the monthly soil
409 temperature instead of a constant value, the thermal recovery efficiency of both options was compared for
410 each sample. Fig. 10 shows that applying a constant temperature at the top results in a consistent
411 underestimation of the efficiency of the ATES system. The difference in recovery efficiency is up to 10 %
412 but decreases significantly to a maximum of 6 % in the second year of operation. There is no link between
413 the predicted efficiency of the ATES system and the difference in efficiency.

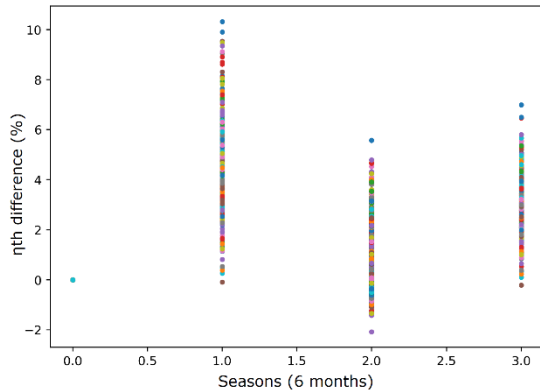


Fig. 10. Difference in thermal recovery efficiency for each model realization when imposing seasonal soil temperature variations instead of imposing a constant top temperature equal to the initial aquifer temperature.

414 The observed difference in efficiency is attributed to the influence of the seasonal fluctuation of the soil
415 temperature on the storage aquifer. To better understand this effect, one sample of each class was selected
416 and simulated with the sine-shape top boundary condition but without the ATES system. The results clearly
417 show that there are temperature fluctuations within the aquifer itself (Fig. 11A, 11B). These fluctuations
418 have an increasing lag and are decreasing in amplitude with depth. This effect results in a slightly higher
419 temperature during the entire year in the lower part of the alluvial aquifer. In the upper part of the alluvial
420 aquifer, it results in a generally higher or lower temperature with the switch occurring roughly in the middle
421 of each 6-month season.

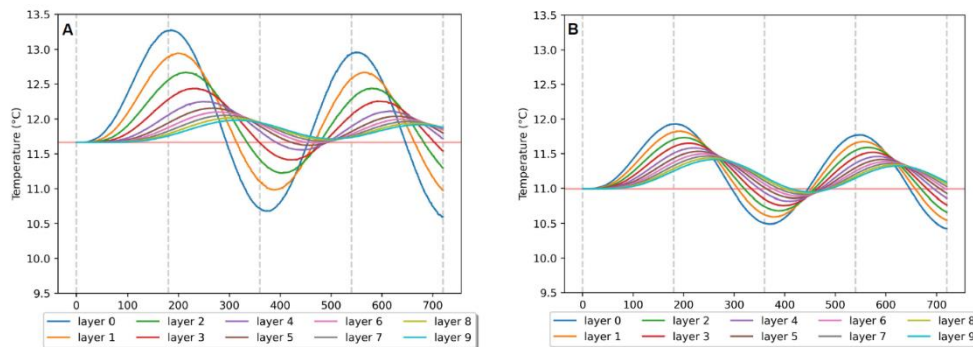


Fig. 11. Natural temperature evolution with time and depth for one model realization of each cluster (A & B). No ATES system was implemented. A sine-shaped temperature profile was imposed reflecting the seasonal soil temperature variations.

422 The fact that there is a difference in recovery efficiency when applying different top boundary conditions
423 even though the sensitivity analyses indicated no sensitivity could have been anticipated. The sensitivity
424 analysis of the temperature evolution over time in the first season of operation already indicated this (Fig.
425 6C). Water was extracted from the cold well area with a different temperature from the initially imposed
426 value which implied that the varying soil temperature influenced the natural aquifer temperature and thus
427 also the ATES efficiency.

428 **5 Discussion**

429 **5.1 Implications for modelling ATES systems**

430 The outcome of the DGSA shows that several model parameters are insensitive to the long-term
431 temperature evolution over time in the warm and cold wells. Specifically, these include the total and effective
432 porosity, the longitudinal dispersivity, the recharge, as well as vertical and horizontal hydraulic conductivity
433 of the least permeable aquifer layer. The total porosity plays an important role in heat transport by
434 conduction through the molecular diffusion coefficient. The longitudinal dispersivity, together with advective
435 transport facilitated by the effective porosity, contributes to heat transport through dispersion processes.
436 Literature reports wide variations in these parameters owing to the diverse nature of aquifers and the
437 questionable accuracy of the estimation through field tests, stemming from uncertain data quality and
438 limited data density (Winter, 2004; Renard, 2007; Fu and Jaime Gómez-Hernández, 2009; Beernink et al.,
439 2022). In shallow aquifers, the recharge rate is also arguable and challenging to estimate due to temporal
440 and spatial variations and dependencies of the runoff on factors such as the percentage of hardened
441 surface, the initial soil saturation, and the rain intensity (Ajami, 2021). Despite considering a broad
442 uncertainty range in the prior, the insensitivity of these variables implies that they can be fixed to average
443 values without significantly influencing the predicted ATES efficiency. Moreover, the consistency of
444 insensitive variables across both cases and previous less general sensitivity studies by Fossoul et al. (2011),
445 Hermans et al. (2018) and Schout et al. (2014) further strengthens this conclusion, affirming the feasibility
446 of using average values to streamline modelling without significantly compromising on prediction accuracy.
447 Fig. 5B and 8B illustrate that the influence of insensitive parameters causes a spread around the

448 relationship between the Darcy flux and efficiency. In other words, the spread represents the possible
449 error/uncertainty associated with this simplification.

450 Furthermore, this study reveals that adopting a top boundary condition mirroring seasonal soil temperature
451 fluctuations impacts the average ambient aquifer temperature up to a depth great enough to impact the
452 thermal recovery efficiency of a shallow ATES system. This influence arises from imposing a consistent
453 5 °C temperature difference between injected water and the natural ambient aquifer temperature while this
454 study shows that the natural aquifer temperature will actually change by the top boundary condition. The
455 analyses with the constant top temperature boundary condition (and thus a constant natural groundwater
456 temperature) cause the efficiency to be systematically underestimated with only a few percentages. In this
457 context, it is important to note that the models assessed worst-case scenarios and in reality, an unsaturated
458 layer is present acting as an insulator, substantially attenuating the impact of the seasonal soil temperature
459 variations. Hence, assuming a constant soil temperature during shallow ATES system modelling is justified.
460 This choice might slightly underestimate the thermal recovery efficiency and is therefore conservative.

461 Nevertheless, this modelled variation in efficiency underscores the importance of accounting for and
462 estimating the initial temperature and temperature fluctuations within the aquifer when assessing the ATES
463 efficiency. These variations might for instance arise from imbalanced ATES systems, leading to overall
464 heating or cooling of the aquifer. Additionally, the presence of urban heat islands could exert an influence,
465 both on shallow and deep layers (Luo and Asproudi, 2015; Schweighofer et al., 2021; Hemmerle et al.,
466 2022; Patton et al., 2024). To our knowledge, this is not yet widely taken into account during feasibility
467 studies for ATES. By acknowledging and understanding the relevant temperature dynamics within the
468 aquifer, ATES system predictions can be refined to better capture real-world conditions and possibly
469 optimize efficiency.

470 Important to mention is that the sensitivity results should always be interpreted considering the sampling
471 method of the prior. For instance, the vertical hydraulic conductivity only emerges as sensitive because it
472 is defined as a ratio from the horizontal hydraulic conductivity in the prior, which is revealed by analyzing
473 the interactions (Fig. 3B).

474 **5.2 Implications for ATES Feasibility Studies**

475 This study identifies the hydraulic conductivity, natural hydraulic gradient and annual storage volume as
476 sensitive parameters which is consistent with the expectations. Knowledge of the sensitive parameters can
477 help optimize future feasibility studies for ATES by focusing field tests to obtain information on parameters
478 that will reduce the uncertainty the most. Accordingly, flux measurements are likely the most efficient, cost-
479 effective and logistically simple strategy. This was confirmed by Hermans et al. (2018) who studied heat
480 tracer tests in the context of an ATES study and revealed that they are efficient in refining the prediction
481 primarily only because of their sensitivity to the hydraulic conductivity and natural gradient (Darcy flux).

482 Novel threshold values for Darcy flux are identified which can be used to classify future potential ATES
483 systems into more efficient, less efficient, and least efficient categories before having to carry out a more
484 detailed case-specific feasibility study. Additionally, the DGSA method with a broad prior uncertainty allows
485 us to gain general insights into the conditions where recovery efficiency will be optimal. It is important to
486 keep in mind that when assessing different classes of thermal recovery efficiency for ATES systems, they
487 should be viewed as relative indicators of the efficiency rather than conclude on absolute values of the
488 expected thermal recovery efficiency. This is because the efficiency of ATES systems typically increases
489 over time as not all injected thermal energy is recovered during the extraction phase. It is only after a certain
490 time of operation (+/- 5 years) that a dynamical equilibrium is achieved. The supplementary materials
491 provide a validation of the results based on the considered shorter simulation time of 3 and 2 cycles for
492 cases 1 and 2 respectively (S4). Moreover, the Darcy flux thresholds only offer a relative indication of
493 efficiency because the calculation of the thermal recovery efficiency is dependent on the flow rate, which
494 fluctuates based on the demand and is therefore also not necessarily equal in the summer and winter
495 seasons.

496 For case 1, the parameter distributions indicate that when the horizontal hydraulic conductivity and gradient
497 are below $2.2E-4$ m/s and 0.12 %, the least efficient storage conditions (within the considered range of
498 uncertainty) will always be avoided (Fig. 4). Still, even for a higher conductivity and/or gradient the ATES
499 system can be highly efficient, as illustrated by the overlap of the parameter ranges of the 3 clusters. In that
500 regard, a Darcy flux measurement is more informative compared to an estimation of the gradient/hydraulic

501 conductivity. Then, it is sufficient to determine whether the estimated darcy flux is lower than 9.5 m/y, higher
502 than 20.5 m/y or in between both thresholds to get a relative idea of the thermal recovery efficiency that
503 can be expected. Nevertheless, even the least efficient class of ATEs systems still holds the potential for
504 significantly contributing to mitigate greenhouse gas emissions compared to conventional heating and
505 cooling systems and they would still outperform alternatives like air source heat pumps. This suggests that
506 the investment in ATEs systems at less optimal locations can still be justified, up to a certain extent, given
507 these advantages (Tas et al., 2023).

508 When examining case 2 the threshold value of the Darcy flux should rather be viewed as a decisive
509 boundary in determining the feasibility of ATEs systems. The least efficient cluster already exhibits a very
510 low thermal recovery efficiency, and it is important to point out that this study did not include lateral
511 heterogeneity in the models which would likely further reduce the efficiency of the system (Sommer et al.,
512 2013; Bloemendal and Hartog, 2018). Therefore, ATEs systems in shallow alluvial aquifers with a natural
513 Darcy flux exceeding $5E-06$ m/s are not advised when aiming for sustainable development of the
514 subsurface in the long term. The results also show that there are only a few favourable combinations of
515 natural gradient and hydraulic conductivity within the gravel layer, indicating a generally lower efficiency of
516 ATEs systems in such aquifers (Fig. 6E). To enhance the system performance in these conditions it is
517 recommended to rather target the upper part of the alluvial aquifer with lower permeability while excluding
518 the lower gravel part, where the natural gradient has a greater adverse impact on the efficiency. This can
519 also be derived when comparing the results of Hermans et al. (2018, 2019) which each targeted a different
520 layer of the alluvial aquifer. Lateral heterogeneity present in alluvial aquifers could also be of advantage by
521 adapting the location for storage to make optimal use of clay lenses that can act as hydraulic barriers
522 (Sommer et al., 2013; Possemiers et al., 2015). Additionally, as suggested by Bloemendal and Olsthoorn
523 (2018), aligning multiple warm and cold wells in these conditions in the direction of groundwater flow can
524 help recover the thermal energy that would otherwise be lost due to the high natural Darcy flux. Despite the
525 existing uncertainty, alluvial aquifers remain interesting targets for ATEs due to their high productivity and
526 low investment cost (shallow drillings) (Robert et al., 2018). Nevertheless, when designing the ATEs system
527 attention should be paid to avoid inundation because the water table is close to the ground surface.

528 It must be emphasized that the derived demarcations linking the Darcy flux to the relative efficiency of ATES
529 systems are applicable specifically for target aquifers falling within the initially defined ranges of the
530 sensitive parameters and it should be pointed out that the thickness of the target aquifers (and for case 1
531 also the storage volume) remained constant throughout the analyses. While conductivity values could
532 potentially be translated to transmissivity, altering the aquifer thickness (or the length of the filter) would
533 inevitably impact the geometry of the storage volume. This, in turn, affects the extent of the thermal losses
534 and consequently the thermal recovery efficiency. Even though the aquifer thickness and, for case 1, the
535 storage volume would be influential parameters they were not included in this study for simplicity. Including
536 these parameters will likely further confirm the outcomes of previous work by Bloemendal and Hartog (2018).
537 As a comparison, plotting the ratio of the thermal radius of influence (R_{th}) and the Darcy flux (u) against
538 the thermal recovery efficiency illustrates that the boundary between the high and medium cluster is located
539 around 1 year (Fig. 12). This is the same as the 80% efficiency line identified by Bloemendal and Hartog
540 (2018).

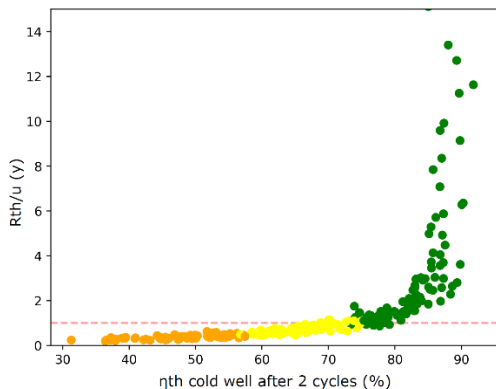


Fig. 12. Relation between the R_{th}/u -ratio and the thermal recovery efficiency with indication of the 1-year line which coincides with the 80 % efficiency threshold established by Bloemendal & Hartog (2018). Model realizations are colored according to their respective cluster.

541 Below this threshold, small changes in the ratio cause large changes in the efficiency meaning that R_{th} has
542 a significant impact on the order of magnitude of the thermal losses for the medium and low clusters. This
543 implies that, for those conditions, losses due to displacement of the storage volume by the ambient
544 groundwater flow velocity are dominant over conduction and dispersion losses. The losses can be more
545 limited when aiming for a less elongated geometry of the storage volume. In the high cluster, dispersion
546 and conduction losses dominate and the efficiency could be further optimized by minimizing the A/V ratio
547 following the guidelines by Bloemendal and Hartog (2018). However, this study does not focus on
548 generating guidelines to optimize ATES well design and recovery efficiency of a single ATES system.
549 Instead, the results provide guidance for decision-making on the feasibility of ATES in the discussed

550 hydrogeological settings, keeping in mind that the storage volume and screened length are operational
551 parameters which could be optimized using the existing guidelines but which in practice also often rely on
552 the available subsurface space, drilling and installation costs, and the energy demand (Bloemendal et al.,
553 2018).

554 **5.3 Future outlook on the application of DGSA and uncertainty quantification for ATES**

555 In Flanders, the initial assessment of the potential for ATES systems is currently mapped according to the
556 transmissivity (AGT (Advanced Groundwater Techniques), 2015). This classification prioritizes the ability
557 to reach a high flow rate and does not indicate the expected efficiency of the ATES system. Based on the
558 insights of this study, it could be beneficial to systematically update this suitability map with Darcy flux
559 measurements. This could offer stakeholders a preliminary estimate of the expected recovery efficiency
560 before committing to and investing in more detailed feasibility studies. Similarly, the existing licensing
561 framework for ATES in Flanders lacks criteria for the minimum efficiency and energy balance that should
562 be reached even though it is of crucial interest when aiming for an optimal distribution of subsurface
563 activities and a sustainable use of the subsurface (Bloemendal et al., 2018; Compernelle et al., 2022). The
564 link between the Darcy flux and the thermal recovery efficiency that was revealed with the sensitivity
565 analysis might have a practical use in this context as well. More specifically, the Darcy flux values could
566 provide substantiated thresholds for licenses when deciding whether or not to grant a permit based on the
567 expected thermal recovery efficiency. A quick analysis of licensed ATES systems in Flanders showed that
568 currently about 75 % of the systems are located in the Miocene aquifer system of which 75 % are in the
569 Diest Formation which was also targeted for this study. This underscores the practicality of the Darcy flux
570 limits that were identified. For target aquifers that significantly deviate in characteristics from the ranges
571 defined in the priors of this paper, conducting an additional sensitivity analysis may be required.

572 In the future, the results of the DGSA will be used as input for studies aiming to improve the design of
573 shallow geothermal systems and to predict the uncertainty of their energy efficiency. For now, this
574 uncertainty quantification is limited to the spreading around the general trend of increasing efficiency with
575 smaller Darcy flux as illustrated in Fig. 5B and Fig. 8B. If there is no (reliable) flux measurement available
576 or there cannot be certainty whether the proposed Darcy flux thresholds will be exceeded, a more advanced

577 uncertainty quantification method should be used taking into account uncertainty on the sensitive
578 parameters. In reality, at an early stage of exploration data is generally available from different sources,
579 this data could be used to refine and update the prior and refine the DGSA (Lopez-Alvis et al., 2019). The
580 available data should also be used to test the validity of the defined prior distribution by analyzing if the
581 prior is able to generate output covering the available observations (Yin et al., 2020). After reducing the
582 model complexity by fixing insensitive variables the long-term behaviour of ATES systems from short-term
583 field tests becomes possible (Hermans et al., 2018). This will offer a thorough and accurate methodology
584 for proper natural resource management and uncertainty quantification while handling the currently growing
585 complexity of data and models as advocated by Ferré (2017).

586 **6 Conclusion**

587 This study validates the use of a distance-based global sensitivity analysis for ATES systems. It shows that
588 assumptions previously accepted with less general studies can also be demonstrated using a broad prior
589 distribution and a DGSA. This supports that, when exploring a particular hydrogeological setting for ATES,
590 it is beneficial to initially still consider the full uncertainty of the model parameters enhancing the
591 generalizability of the results.

592 Specifically, this study provides a substantiated basis for fixing insensitive model parameters to average
593 values in the studied hydrogeological settings. These parameters include the total and effective porosity,
594 the longitudinal dispersivity, the recharge, and both vertical and horizontal hydraulic conductivity of the least
595 permeable part of the aquifer. This study distinguishes itself from previous sensitivity analyses by showing
596 that the uncertainty that will result from these simplifications can be viewed as the limited interval of thermal
597 recovery efficiency values that are still considered possible if a precise flux measurement is available.

598 The DGSA results also enhance our understanding of how surface temperature fluctuations impact the
599 storage of thermal energy in very shallow aquifers. It proves that while these fluctuations do influence
600 aquifer temperature and thus the ATES efficiency, model simplifications not accounting for soil temperature
601 fluctuations are justified. Further, vertical thermal losses are counterbalanced by gains and they can be
602 attributed to the functioning of the ATES system itself. This is a valuable outcome, indicating that, although

603 software exists to include all relevant heat transfer processes in the saturated and unsaturated shallow
604 subsurface, it is not necessary to implement them in the context of ATES.

605 The parameters with major influence on the efficiency are the hydraulic conductivity, the natural hydraulic
606 gradient and the annual storage volume. While this confirms the results of previous less general studies,
607 this study further identifies Darcy flux thresholds that can serve when deciding upon the investment in ATES
608 systems. In thick productive settings for ATES, a flux lower than 9.5 m/y indicates a very efficient system
609 while a flux higher than 20.5 m/y characterizes the least favorable conditions. In shallow alluvial aquifers,
610 ATES systems should not be implemented when Darcy fluxes are higher than 160 m/y because this will
611 cause the system to be highly inefficient in terms of thermal recovery. As such, in a cost-efficient and
612 logistically simple way, these flux measurements can provide a first measure of the ATES system's
613 efficiency before carrying out a more detailed study.

614 For the two studied settings, new insights were also gained into the conditions where the recoverability of
615 the stored thermal energy is optimal. A relatively low hydraulic conductivity and gradient will lead to a high
616 recovery efficiency but these conditions are not a requirement. In this sense, flux measurements that
617 account for both properties together, are more informative to identify favorable conditions.

618 In summary, this study shows that the DGSA method is effective in the context of ATES. It can serve to
619 identify the sensitivity of model parameters, to reduce the model complexity without significantly reducing
620 the uncertainty and to gain an understanding of the recovery efficiency and heat transport processes in
621 different hydrogeological settings. This is crucial considering the tendency to target less known and less
622 favourable aquifers and the aim for uncertainty quantification. The nuanced understanding gained from this
623 study contributes to the optimization of ATES systems, offering practical guidance for more efficient
624 feasibility studies and decision-making based on sound scientific approaches.

625 **CRedit authorship contribution statement**

626 **Luka Tas:** Conceptualization, Methodology, Software, Visualization, Data curation, Validation, Formal
627 analysis, Investigation, Writing – original draft, Writing – review & editing, Funding acquisition. **Niels**

628 **Hartog:** Conceptualization, Methodology, Supervision, Writing – review and editing. **Martin Bloemendal:**

**This is a non-peer-reviewed preprint submitted to EarthArXiv.
It is under review in Geothermal Energy.**

629 Conceptualization, Supervision, Writing – review and editing, Methodology. **David Simpson:** Resources,
630 Conceptualization, Supervision, Methodology, Writing – review and editing. **Tanguy Robert:** Resources,
631 Writing – review and editing. **Robin Thibaut:** Software, Resources, Writing – review and editing. **Le Zhang:**
632 Methodology, Writing – review and editing. **Thomas Hermans:** Writing – review and editing, Supervision,
633 Funding acquisition, Conceptualization, Methodology, Investigation, Formal analysis.

634 **Declaration of Competing Interest**

635 On behalf of all authors, the corresponding author states that there is no known conflict of interest that could
636 have influenced the work reported in this paper.

637 **Acknowledgements and funding**

638 This work has received funding from the BOF (*bijzonder onderzoeksfonds* - special research fund)
639 fellowship from Ghent University (grant number: 01D03222) and an FWO (Research Foundation Flanders)
640 grant for a 2-month research stay at the KWR water research institute in Nieuwegein (The Netherlands)
641 further promoted this research (grant number: V430223N). Later, Luka Tas became an SB (strategic basic
642 research) PhD fellow, fully funded by FWO (grant number: 1SH0M24N). The resources and services used
643 in this work were provided by the VSC (Flemish Supercomputer Center), funded by the Research
644 Foundation - Flanders (FWO) and the Flemish Government and the strategic basic research project
645 DIAMONDS (grant number S001324N). We would like to express our sincere thanks to the colleagues at
646 KWR for their help with numerical problems and the warm welcome. Finally, we truly appreciate the
647 members of the DIAMONDS project team for the fruitful discussions and for offering new perspectives on
648 the sustainable use of the subsurface.

649 **Availability of data and materials**

650 The input and output data of the simulations generated and used for the DGSA's of this study are openly
651 available on Zenodo <https://doi.org/10.5281/zenodo.13347760>. The scripts used to process the input and
652 output are available on GitHub https://github.com/lukatas/ATES_SensitivityAnalyses.git

653 (<https://doi.org/10.5281/zenodo.13349645>). The online version of the publication contains the
654 supplementary material.

655 **References**

656 AGT (Advanced Groundwater Techniques). KWO potentieel in Vlaanderen: Kaart – Versie 3. AGTref.:
657 2015/C/01-1728-03 mp/jvs 09/10/15. Aartselaar: 2015.

658 Ajami H. Geohydrology: Groundwater. *Encycl. Geol.*, Elsevier; 2021, p. 408–15.
659 <https://doi.org/10.1016/B978-0-12-409548-9.12388-7>.

660 Bakker M, Post V, Langevin CD, Hughes JD, White JT, Starn JJ, et al. Scripting MODFLOW Model
661 Development Using Python and FloPy. *Groundwater* 2016;54:733–9. <https://doi.org/10.1111/gwat.12413>.

662 Batlle-Aguilar J, Brouyère S, Dassargues A, Morasch B, Hunkeler D, Höhener P, et al. Benzene dispersion
663 and natural attenuation in an alluvial aquifer with strong interactions with surface water. *J Hydrol*
664 2009;369:305–17. <https://doi.org/10.1016/j.jhydrol.2009.02.014>.

665 Bedekar V, Morway ED, Langevin CD, Tonkin MJ. MT3D-USGS: Groundwater Solute Transport Simulator
666 for MODFLOW 2016. <https://doi.org/10.5066/F75T3HKD>.

667 Beernink S, Barnhoorn A, Vardon P, Bloemendal M, Hartog N. Impact of vertical layering and the
668 uncertainty and anisotropy of hydraulic conductivity on HT-ATES performance. 2022.

669 Beernink S, Hartog N, Vardon PJ, Bloemendal M. Heat losses in ATES systems: The impact of processes,
670 storage geometry and temperature. *Geothermics* 2024;117:102889.
671 <https://doi.org/10.1016/j.geothermics.2023.102889>.

672 Bloemendal M, Hartog N. Analysis of the impact of storage conditions on the thermal recovery efficiency of
673 low-temperature ATES systems. *Geothermics* 2018;71:306–19.
674 <https://doi.org/10.1016/j.geothermics.2017.10.009>.

- 675 Bloemendal M, Jaxa-Rozen M, Olsthoorn T. Methods for planning of ATEs systems. *Appl Energy*
676 2018;216:534–57. <https://doi.org/10.1016/j.apenergy.2018.02.068>.
- 677 Bloemendal M, Olsthoorn T. ATEs systems in aquifers with high ambient groundwater flow velocity.
678 *Geothermics* 2018;75:81–92. <https://doi.org/10.1016/j.geothermics.2018.04.005>.
- 679 Bridger D, Allen D. Heat transport simulations in a heterogeneous aquifer used for aquifer thermal energy
680 storage (ATEs). *Can Geotech J* 2010;47:96–115. <https://doi.org/10.1139/T09-078>.
- 681 Claesson J, Eskilson P. Conductive heat extraction to a deep borehole: Thermal analyses and dimensioning
682 rules. *Energy* 1988;13:509–27. [https://doi.org/10.1016/0360-5442\(88\)90005-9](https://doi.org/10.1016/0360-5442(88)90005-9).
- 683 Compennolle T, Eswaran A, Welkenhuysen K, Hermans T, Walraevens K, Van Camp M, et al. Towards a
684 dynamic and sustainable management of geological resources. *Geol Soc Lond Spec Publ* 2022;528.
685 <https://doi.org/10.1144/SP528-2022-75>.
- 686 Databank Ondergrond Vlaanderen (Database Underground Flanders). Verkenner (Explorer) n.d.
- 687 Davies DL, Bouldin DW. A Cluster Separation Measure. *IEEE Trans Pattern Anal Mach Intell* 1979;PAMI-
688 1:224–7. <https://doi.org/10.1109/TPAMI.1979.4766909>.
- 689 De Paoli C, Duren T, Petitclerc E, Agniel M, Dassargues A. Modelling Interactions between Three Aquifer
690 Thermal Energy Storage (ATEs) Systems in Brussels (Belgium). *Appl Sci* 2023;13:2934.
691 <https://doi.org/10.3390/app13052934>.
- 692 De Schepper G, Bolly P-Y, Vizzotto P, Wecxsteen H, Robert T. Investigations into the First Operational
693 Aquifer Thermal Energy Storage System in Wallonia (Belgium): What Can Potentially Be Expected?
694 *Geosciences* 2020;10:33. <https://doi.org/10.3390/geosciences10010033>.
- 695 De Schepper G, Paulus C, Bolly P-Y, Hermans T, Lesparre N, Robert T. Assessment of short-term aquifer
696 thermal energy storage for demand-side management perspectives: Experimental and numerical
697 developments. *Appl Energy* 2019;242:534–46. <https://doi.org/10.1016/j.apenergy.2019.03.103>.

- 698 Doughty C, Hellström G, Tsang CF, Claesson J. A dimensionless parameter approach to the thermal
699 behavior of an aquifer thermal energy storage system. *Water Resour Res* 1982;18:571–87.
700 <https://doi.org/10.1029/WR018i003p00571>.
- 701 Duijff R, Bloemendal M, Bakker M. Interaction Effects Between Aquifer Thermal Energy Storage Systems.
702 *Groundwater* 2021;61:173–82. <https://doi.org/10.1111/gwat.13163>.
- 703 Farmer WH, Vogel RM. On the deterministic and stochastic use of hydrologic models. *Water Resour Res*
704 2016;52:5619–33. <https://doi.org/10.1002/2016WR019129>.
- 705 Fenwick D, Scheidt C, Caers J. Quantifying Asymmetric Parameter Interactions in Sensitivity Analysis:
706 Application to Reservoir Modeling. *Math Geosci* 2014;46:493–511. [https://doi.org/10.1007/s11004-014-](https://doi.org/10.1007/s11004-014-9530-5)
707 9530-5.
- 708 Ferguson G. Heterogeneity and Thermal Modeling of Ground Water. *Groundwater* 2007;45:485–90.
709 <https://doi.org/10.1111/j.1745-6584.2007.00323.x>.
- 710 Ferré TPA. Revisiting the Relationship Between Data, Models, and Decision-Making. *Groundwater*
711 2017;55:604–14. <https://doi.org/10.1111/gwat.12574>.
- 712 Fleuchaus P, Godschalk B, Stober I, Blum P. Worldwide application of aquifer thermal energy storage – A
713 review. *Renew Sustain Energy Rev* 2018;94:861–76. <https://doi.org/10.1016/j.rser.2018.06.057>.
- 714 Fossoul F, Orban P, Dassargues A. Numerical simulation of heat transfer associated with low enthalpy
715 geothermal pumping in an alluvial aquifer. *Geol Belg* 2011.
- 716 Fu J, Jaime Gómez-Hernández J. Uncertainty assessment and data worth in groundwater flow and mass
717 transport modeling using a blocking Markov chain Monte Carlo method. *J Hydrol* 2009;364:328–41.
718 <https://doi.org/10.1016/j.jhydrol.2008.11.014>.
- 719 Gao L, Zhao J, An Q, Wang J, Liu X. A review on system performance studies of aquifer thermal energy
720 storage. *Energy Procedia* 2017;142:3537–45. <https://doi.org/10.1016/j.egypro.2017.12.242>.

- 721 Harbaugh AW, Langevin CD, Hughes JD, Niswonger RG, Konikow LF. MODFLOW-2005: USGS three-
722 dimensional finite-difference groundwater model 2017. <https://doi.org/10.5066/F7RF5S7G>.
- 723 Hecht-Méndez J, Molina-Giraldo N, Blum P, Bayer P. Evaluating MT3DMS for Heat Transport Simulation
724 of Closed Geothermal Systems. *Groundwater* 2010;48:741–56. [https://doi.org/10.1111/j.1745-
725 6584.2010.00678.x](https://doi.org/10.1111/j.1745-6584.2010.00678.x).
- 726 Heldt S, Beyer C, Bauer S. Uncertainty assessment of thermal recovery and subsurface temperature
727 changes induced by high-temperature aquifer thermal energy storage (HT-ATES): A case study.
728 *Geothermics* 2024;122:103086. <https://doi.org/10.1016/j.geothermics.2024.103086>.
- 729 Hemmerle H, Ferguson G, Blum P, Bayer P. The evolution of the geothermal potential of a subsurface
730 urban heat island. *Environ Res Lett* 2022;17:084018. <https://doi.org/10.1088/1748-9326/ac7e60>.
- 731 Hermans T, Goderniaux P, Jougnot D, Fleckenstein JH, Brunner P, Nguyen F, et al. Advancing
732 measurements and representations of subsurface heterogeneity and dynamic processes: towards 4D
733 hydrogeology. *Hydrol Earth Syst Sci* 2023;27:255–87. <https://doi.org/10.5194/hess-27-255-2023>.
- 734 Hermans T, Lesparre N, de Schepper G, Robert T. Bayesian evidential learning: a field validation using
735 push-pull tests. *Hydrogeol J* 2019;27:1661–72. <https://doi.org/10.1007/s10040-019-01962-9>.
- 736 Hermans T, Nguyen F, Klepikova M, Dassargues A, Caers J. Uncertainty Quantification of Medium-Term
737 Heat Storage From Short-Term Geophysical Experiments Using Bayesian Evidential Learning. *Water
738 Resour Res* 2018;54:2931–48. <https://doi.org/10.1002/2017WR022135>.
- 739 Hoffmann R, Dassargues A, Goderniaux P, Hermans T. Heterogeneity and Prior Uncertainty Investigation
740 Using a Joint Heat and Solute Tracer Experiment in Alluvial Sediments. *Front Earth Sci* 2019;7.
741 <https://doi.org/10.3389/feart.2019.00108>.
- 742 Hoteit H, He X, Yan B, Vahrenkamp V. Uncertainty quantification and optimization method applied to time-
743 continuous geothermal energy extraction. *Geothermics* 2023;110:102675.
744 <https://doi.org/10.1016/j.geothermics.2023.102675>.

- 745 Hughes JD, Langevin CD, Paulinski SR, Larsen JD, Brakenhoff D. FloPy Workflows for Creating Structured
746 and Unstructured MODFLOW Models. *Groundwater* 2024;62:124–39. <https://doi.org/10.1111/gwat.13327>.
- 747 Jackson MD, Regnier G, Staffell I. Aquifer Thermal Energy Storage for low carbon heating and cooling in
748 the United Kingdom: Current status and future prospects. *Appl Energy* 2024;376:124096.
749 <https://doi.org/10.1016/j.apenergy.2024.124096>.
- 750 Jeon J-S, Lee S-R, Pasquinelli L, Fabricius IL. Sensitivity analysis of recovery efficiency in high-temperature
751 aquifer thermal energy storage with single well. *Energy* 2015;90:1349–59.
752 <https://doi.org/10.1016/j.energy.2015.06.079>.
- 753 Kaufman L, Rousseuw PJ. *Review of Finding Groups in Data: An Introduction to Cluster Analysis*. 1990.
754 <https://doi.org/10.2307/2532178>.
- 755 Klepikova M, Wildemeersch S, Hermans T, Jamin P, Orban P, Nguyen F, et al. Heat tracer test in an alluvial
756 aquifer: Field experiment and inverse modelling. *J Hydrol* 2016;540:812–23.
757 <https://doi.org/10.1016/j.jhydrol.2016.06.066>.
- 758 Kurylyk BL, MacQuarrie KTB, Caissie D, McKenzie JM. Shallow groundwater thermal sensitivity to climate
759 change and land cover disturbances: derivation of analytical expressions and implications for stream
760 temperature modeling. *Hydrol Earth Syst Sci* 2015;19:2469–89. <https://doi.org/10.5194/hess-19-2469-2015>.
- 761 Lopez-Alvis J, Hermans T, Nguyen F. A cross-validation framework to extract data features for reducing
762 structural uncertainty in subsurface heterogeneity. *Adv Water Resour* 2019;133:103427.
763 <https://doi.org/10.1016/j.advwatres.2019.103427>.
- 764 Lu D, Ricciuto D. Efficient Distance-based Global Sensitivity Analysis for Terrestrial Ecosystem Modeling.
765 2020 *Int. Conf. Data Min. Workshop ICDMW, Sorrento, Italy: IEEE; 2020, p. 324–32*.
766 <https://doi.org/10.1109/ICDMW51313.2020.00052>.

- 767 Luo Z, Asproudi C. Subsurface urban heat island and its effects on horizontal ground-source heat pump
768 potential under climate change. *Appl Therm Eng* 2015;90:530–7.
769 <https://doi.org/10.1016/j.applthermaleng.2015.07.025>.
- 770 Ma R, Zheng C. Effects of Density and Viscosity in Modeling Heat as a Groundwater Tracer. *Groundwater*
771 2010;48:380–9. <https://doi.org/10.1111/j.1745-6584.2009.00660.x>.
- 772 Park J, Yang G, Satija A, Scheidt C, Caers J. DGSA: A Matlab toolbox for distance-based generalized
773 sensitivity analysis of geoscientific computer experiments. *Comput Geosci* 2016;97:15–29.
774 <https://doi.org/10.1016/j.cageo.2016.08.021>.
- 775 Patton A, Cleall P, Cuthbert M. Identifying urban subsurface thermal and hydraulic processes from time-
776 series groundwater temperature data. *Copernicus Meetings; 2024*. [https://doi.org/10.5194/egusphere-](https://doi.org/10.5194/egusphere-egu24-1319)
777 [egu24-1319](https://doi.org/10.5194/egusphere-egu24-1319).
- 778 Possemiers M, Huysmans M, Batelaan O. Application of multiple-point geostatistics to simulate the effect
779 of small-scale aquifer heterogeneity on the efficiency of aquifer thermal energy storage. *Hydrogeol J*
780 2015;23:971–81. <https://doi.org/10.1007/s10040-015-1244-3>.
- 781 Poulsen SE, Balling N, Nielsen SB. A parametric study of the thermal recharge of low enthalpy geothermal
782 reservoirs. *Geothermics* 2015;53:464–78. <https://doi.org/10.1016/j.geothermics.2014.08.003>.
- 783 Preene M, Powrie W. Ground energy systems: from analysis to geotechnical design. *Géotechnique*
784 2009;59:261–71. <https://doi.org/10.1680/geot.2009.59.3.261>.
- 785 Ramos-Escudero A, García-Cascales MS, Urchueguía JF. Evaluation of the Shallow Geothermal Potential
786 for Heating and Cooling and Its Integration in the Socioeconomic Environment: A Case Study in the Region
787 of Murcia, Spain. *Energies* 2021;14:5740. <https://doi.org/10.3390/en14185740>.
- 788 Renard P. Stochastic Hydrogeology: What Professionals Really Need? *Groundwater* 2007;45:531–41.
789 <https://doi.org/10.1111/j.1745-6584.2007.00340.x>.

- 790 Robert T, Hermans T, Lesparre N, De Schepper G, Nguyen F, Defourny A, et al. Towards a subsurface
791 predictive-model environment to simulate aquifer thermal energy storage for demand-side management
792 applications. Proc. SSB 2018 10th Int. Conf. Syst. Simul. Build., 2018.
- 793 Scheidt C, Li L, Caers J. Quantifying Uncertainty in Subsurface Systems. 1st ed. Wiley; 2018.
794 <https://doi.org/10.1002/9781119325888>.
- 795 Schout G, Drijver B, Gutierrez-Neri M, Schotting R. Analysis of recovery efficiency in high-temperature
796 aquifer thermal energy storage: a Rayleigh-based method. Hydrogeol J 2014;22:281–91.
797 <https://doi.org/10.1007/s10040-013-1050-8>.
- 798 Schweighofer JAV, Wehrl M, Baumgärtel S, Rohn J. Detecting Groundwater Temperature Shifts of a
799 Subsurface Urban Heat Island in SE Germany. Water 2021;13:1417. <https://doi.org/10.3390/w13101417>.
- 800 Sommer W, Valstar J, van Gaans P, Grotenhuis T, Rijnaarts H. The impact of aquifer heterogeneity on the
801 performance of aquifer thermal energy storage. Water Resour Res 2013;49:8128–38.
802 <https://doi.org/10.1002/2013WR013677>.
- 803 Stemmler R, Blum P, Schüppler S, Fleuchaus P, Limoges M, Bayer P, et al. Environmental impacts of
804 aquifer thermal energy storage (ATES). Renew Sustain Energy Rev 2021;151:111560.
805 <https://doi.org/10.1016/j.rser.2021.111560>.
- 806 Tas L, Simpson D, Hermans T. Assessing the potential of low-transmissivity aquifers for aquifer thermal
807 energy storage systems: a case study in Flanders (Belgium). Hydrogeol J 2023;31:2363–80.
808 <https://doi.org/10.1007/s10040-023-02696-5>.
- 809 Wildemeersch S, Jamin P, Orban P, Hermans T, Klepikova M, Nguyen F, et al. Coupling heat and chemical
810 tracer experiments for estimating heat transfer parameters in shallow alluvial aquifers. J Contam Hydrol
811 2014;169:90–9. <https://doi.org/10.1016/j.jconhyd.2014.08.001>.
- 812 Winston RB. ModelMuse Version 5.1.1 2022. <https://doi.org/10.5066/P90QQ94D>.

813 Winter CL. Stochastic hydrology: practical alternatives exist. *Stoch Environ Res Risk Assess* 2004;18:271–
814 3. <https://doi.org/10.1007/s00477-004-0198-0>.

815 Yin Z, Strebelle S, Caers J. Automated Monte Carlo-based quantification and updating of geological
816 uncertainty with borehole data (AutoBEL v1.0). *Geosci Model Dev* 2020;13:651–72.
817 <https://doi.org/10.5194/gmd-13-651-2020>.

818 Zeghici RM, Oude Essink GHP, Hartog N, Sommer W. Integrated assessment of variable density–viscosity
819 groundwater flow for a high temperature mono-well aquifer thermal energy storage (HT-ATES) system in a
820 geothermal reservoir. *Geothermics* 2015;55:58–68. <https://doi.org/10.1016/j.geothermics.2014.12.006>.

821 Zhang L, Dieudonné A-C, Daniilidis A, Dong L, Cao W, Thibaut R, et al. Thermo-Hydro-Mechanical
822 Modeling of Geothermal Energy Systems in Deep Mines: Uncertainty Quantification and Design
823 Optimization 2024.

824 Zuurbier KG, Hartog N, Valstar J, Post VEA, van Breukelen BM. The impact of low-temperature seasonal
825 aquifer thermal energy storage (SATES) systems on chlorinated solvent contaminated groundwater:
826 Modeling of spreading and degradation. *J Contam Hydrol* 2013;147:1–13.
827 <https://doi.org/10.1016/j.jconhyd.2013.01.002>.

828